ISOTHERMAL AND THERMOMECHANICAL FATIGUE OF SUPERALLOY C263

Y.H. Zhang and D.M. Knowles

Rolls Royce University Technology Centre
Department of Materials Science and Metallurgy
University of Cambridge, England

Abstract

A study has been conducted to examine the behaviour of isothermal low cycle fatigue (LCF) and thermomechanical fatigue (TMF) of Ni-base superalloy C263 over a temperature regime from 25 to 950°C for several strain ranges. The macroscopic performance was correlated by detailed microstructural analysis using TEM and SEM. Initial cyclic hardening in isothermal LCF occurred at all temperatures. At room temperature, slight cyclic softening occurred following the hardening stage. This effect is more evident with increasing strain amplitude. TEM analysis revealed that this was related to dislocation shearing of γ' precipitates. Continuous cyclic hardening and considerable softening were observed respectively at 600 and 800°C. As at room temperature, planar slip was pronounced, but more slip systems operated resulting in a higher dislocation density as temperature increased. A gradual change of fracture mode from planar transgranular at room temperature to more wavy tansgranular failure at 800°C was observed. At 950°C, the load carrying capacity of C263 alloy was significantly reduced and the material was essentially cyclically stable. During LCF at this temperature, carbides precipitate in the matrix, promoted by plastic deformation, while the γ' phase was dissolved. IP and OP TMF tests suggested that considerable high temperature creep deformation occurred followed by heavy plastic deformation at low temperatures. Plastic recovery and recrystallization produced a microstructure with elongated grains and subgrains which is different from that in isothermal fatigue. In all TMF tests and isothermal LCF at 950°C, fracture was predominantly via an intergranular mechanism.

Superalloys 2000
. Edited by T.M. Pollock, R.D. Kissinger, R.R. Bowman,
K.A. Green, M. McLean, S. Olson, and J.J. Schirra
TMS (The Minerals, Metals & Materials Society), 2000

Introduction

Nimonic C263 is a polycrystalline Ni-base superalloy that is solid solution strengthened by chromium, cobalt, molybdenum and $Ni_3(Ti,Al)$ γ' precipitates. It is widely used in stationary components such as combustion chamber, casing, liner, exhaust ducting and bearing housing in aeroengines. The choice of this material is based primarily on a combination of excellent fabricability, weldability and good resistance to oxidation [1]. When it is used in combustion chambers, it suffers from cyclic thermal and mechanical stresses during the start-up, steady-state and shut-down operations. Furthermore, standard laboratory isothermal testing can not include all the damage and failure processes that may occur under service conditions [2,3]. One example of such changes is the high temperature recovery of plastic deformation introduced at lower temperatures.

In recent years, there has been an increasing interest in combustor lifing. Combustor lifing differs markedly from blades and discs because the material can creep to such an extent at the high temperature end of the cycle that the residual stress at low temperatures causes severe deformation by plasticity. Therefore, the lifing for combustors represents challenges not seen for turbine aerofoil and disc materials.

In order to generate physically realistic constitutive equations for C263 combustor material, a comprehensive understanding of both macroscopic cyclic fatigue behaviour and microscopic deformation and fracture mechanisms under LCF and TMF is essential. Currently, the research in this field for this material is limited in the open literature.

Materials and Experiments

The C263 alloy was provided by Rolls-Royce plc as 21.0mm diameter bars in a standard heat treatment. This treatment involves solution at 1150°C for 2 h, quenching in water and ageing at 800°C for 8h followed by air cooling. Microstructural observation revealed that the material has a mean-linear-intercept grain size of about 104 μm, an average γ' precipitate size of about 22 nm, a small quantity of undissolved primary MC carbides and many annealing twins. Fine discontinuous $M_{23}C_6$ carbides are present along grain and twin boundaries and are coherent with the neighbouring grains. The chemical composition of the alloy is given in Table 1.

Fully-reversed (R=-1), total axial strain controlled isothermal LCF tests were carried out on 6.4mm dia. and 14.0 mm parallel gauge length specimens at temperatures in the range 25°C to 950°C. A symmetric 0.25 Hz trapezoidal cyclic waveform with 1 second ramps and holds was used. The axial strain ranges were from 0.5% to 2.0%. TMF tests were performed under total strain control on a computer controlled, servohydraulic test system with a load cell capacity of 50 kN. TMF specimens in the form of hollow cylindrical test-pieces having a gauge length of 12.5 mm, external diameter of 6.4 mm and a wall thickness of 1.0 mm were heated by an induction coil and cooled by forced air to achieve linear heating and cooling rates. In-phase (IP) and out-of-phase (OP) TMF tests were conducted with a cycle period of 130 seconds: 45 seconds for heating up and 85 seconds for cooling down. The temperature limits were T_{min}=300°C and T_{max}=950°C with a mechanical strain range, $\Delta\varepsilon$, of 0.6% and strain ratio R=0 for IP and R=- ∞ for OP TMF tests. IP and OP are defined in Fig. 1. Strains and temperatures were monitored by contacting extensometry and optical pyrometry, respectively. The thermal expansion for the material was first recorded under zero load in order that it could be subtracted from the total strain during testing in order to impose a given mechanical strain.

Table 1. Nominal compositions (wt. %) of C263 alloy.

Ni	Co	Cr	Fe	Mo	Mn	Si	Ti	Al	C
Bal.	20	20	0.7	5.8	0.6	0.4	2.15	0.45	0.06

Both as-received material and some selected tested specimens were examined in a scanning electron microscope (SEM) and a transmission electron microscope (TEM) to identify the deformation and damage mechanisms. For isothermal LCF specimens, TEM foils were sliced along a plane vertical to the loading direction, while for TMF, the OP specimen was sectioned along the plane parallel to the loading direction. TEM foils were examined in a JEOL 2000 FX electron microscope with an operating voltage of 200 kV.

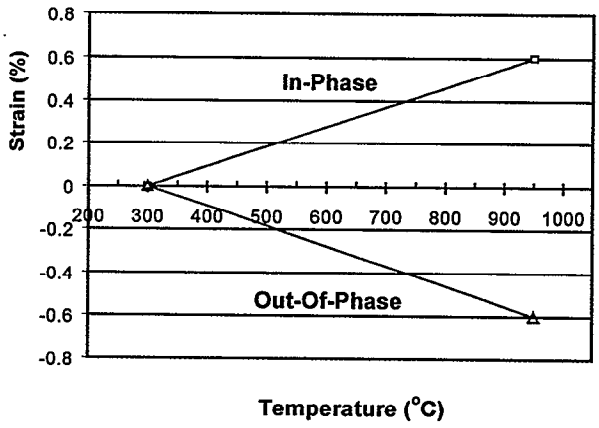

Figure 1: Schematic showing the definition of IP and OP TMF and the temperature and strain ranges applied.

Results and Discussion

Isothermal LCF

Table 2 summarises the isothermal LCF and TMF test results. Fig. 2 shows the influence of temperature on peak stress and fatigue lives when compared at a strain range of 0.75% (since tests were carried out at R=-1 and tensile and compressive stresses exhibited symmetry, only the maximum tensile stresses developed during isothermal LCF are plotted). All specimens initially exhibited cyclic hardening. At lower temperatures it took longer to reach a given saturated stress range. At room temperature, the specimen exhibited slight softening following the cyclic hardening stage. At 600°C, a consistent, moderate cyclic hardening was observed before crack initiation and propagation.

When the temperature was increased to 800°C, the initial maximum stresses were comparable with that at 600°C during hardening stage, but a significant softening then followed. At 950°C, a short period of limited hardening followed by very gradual cyclic softening can be seen with the general load carrying capacity significantly decreased. The hysteresis loops of strain against stress of the first 10 cycles were shown in Fig. 3 where it can be seen that significant creep deformation occurred near both strain extremes.

Generally, the shape and evolution of the stress/strain hysteresis LCF curves of C263 alloy are more dependent on temperature than strain range. The general features of the deformation such as cyclic hardening/softening and creep at each temperature were not affected by strain range, but the magnitudes of hardening or softening behaviour have been found to be dependent on the range, especially at room temperature as shown in Fig. 4. At this temperature, with increasing strain range, cyclic softening begins earlier and is more evident. When the strain range was increased to 2.0%, a marked cyclic hardening followed by softening can be seen. This is in agreement with the work on Nimonic 90 superalloy [4] where increasing strain range resulted in earlier cyclic softening and higher stress maximum at room temperature.

Table 2. The isothermal LCF and TMF testing conditions and results.

Specimen No	Temperature (°C)	Strain range (%)	Cycles to failure
LCF123	20	0.75	6250
LCF132	20	1.00	5090
LCF142	20	2.00	600
LCF221	600	0.75	2985
LCF232	600	1.00	1333
LCF241	600	1.50	360
LCF311	800	0.50	3680
LCF321	800	0.75	1059
LCF331	800	0.90	680
LCF411	950	0.50	800
LCF421	950	0.75	390
IP TMF	300-950	0.60	280
OP TMF	300-950	0.60	210

Thermomechanical Fatigue

Each TMF test started from the lower temperature and a shake-down or shake-up of stresses occurred. Stress-strain response was stabilised once the temperature reached and passed the maximum temperature in the first cycle. This implies that the initial strain R ratio will not play a significant role in the subsequent stress-strain behaviour in the TMF test provided little damage occurred in the first cycle. When approaching the maximum temperature, both tensile and compressive stresses dropped significantly to much less than the maximum tensile and compressive stresses experienced in the isothermal fatigue at 950°C. A typical temperature-stress hysteresis loop for each type of TMF test is shown in Fig. 5. At certain temperature ranges, especially during cooling from high temperature, a stress fluctuation was seen. This stress discontinuity is considered to be the effect of dynamic strain ageing resulting from interaction between dislocations and diffusing alloying atoms [2]. This phenomenon was not observed during isothermal fatigue tests.

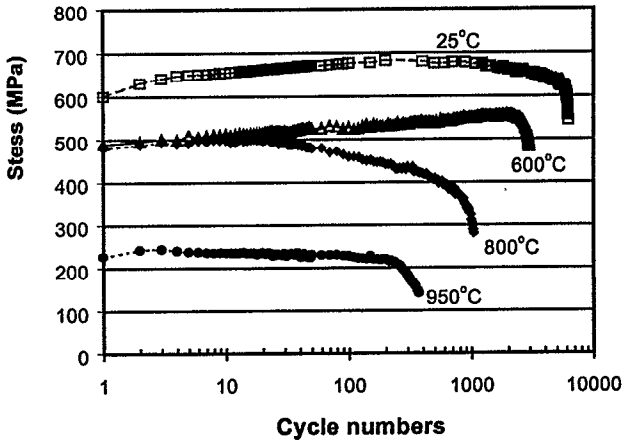

Figure 2: Development of the maximum tensile stresses with increasing cycle numbers at several temperatures, Δε=0.75%.

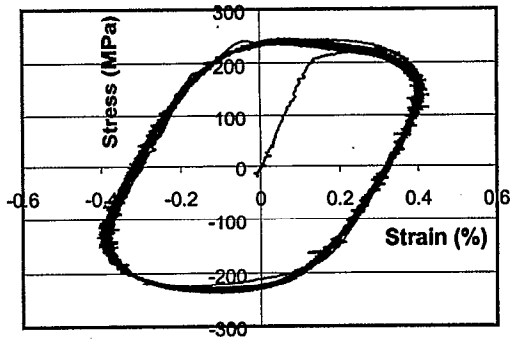

Figure 3: Cyclic hysteresis loops of strain against stress at 950°C, showing creep deformation under tensile and compressive loads.

Microstructural analysis

Isothermal LCF After fatigue failure, several specimens, covering different temperature and strain ranges, were prepared for microstructural analysis. Generally, dislocation density increases with increasing strain ranges. Stacking faults have also been observed in all specimens tested from 25°C to 800°C. In addition, both dislocation and grain boundary structure were strongly influenced by temperature.

Typical TEM microstructures obtained at different temperatures but similar strain ranges are compared in Fig. 6. At room temperature it was found that slip was predominantly planar and concentrated in local parallel slip bands which have the highest resolved shear stress. To investigate the reason for cyclic softening at room temperature, detailed TEM analysis was carried out on the γ′ morphology near the deformed region. Away from the plastic

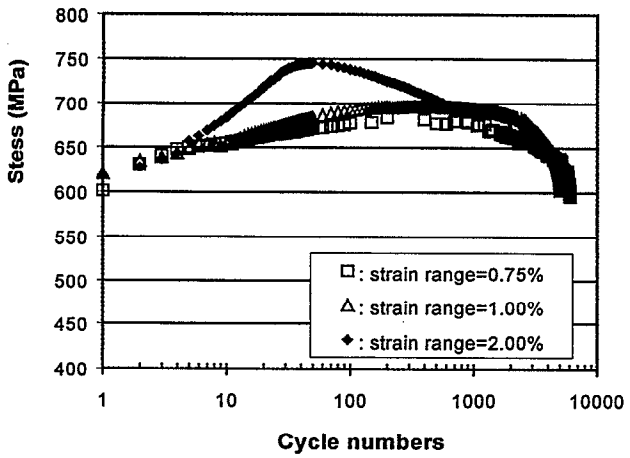

Figure 4: Comparison of maximum tensile stresses with cycle numbers at three strain ranges at room temperature. They exhibit cyclic hardening followed by cyclic softening.

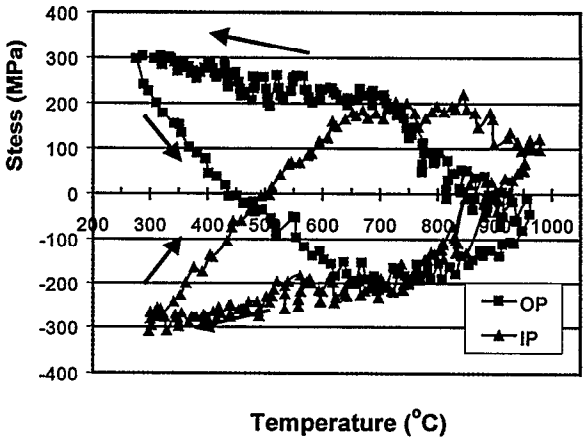

Figure 5: Typical stress-temperature hysteresis loops during IP and OP TMF (taken from the 20th cycle).

deformation area, the γ′ precipitate morphology was unchanged and still exhibited a round shape; but within the slip bands, it was often found that γ′ phase was sheared by dislocation movements, see Fig. 7. This might be linked with the cyclic softening at room temperature. It suggests that repetitive cutting of the fine precipitates by the motion of dislocations results in the reduction in the size of γ′ and gradual cyclic softening. This phenomenon has also been observed in Nimonic alloys PE16 [5], Nimonic 80 [6] and Nimonic 90 [4] and was attributed to the shearing of γ′ precipitates by dislocations during cyclic fatigue at room temperature. Cyclic stress response depends on the internal resistance to deformation of a material. This resistance comes from pinning of dislocation movements by either other dislocations (work hardening) and/or particles (precipitation hardening). When the dislocation structure reaches a saturated state, the reducing resistance to deformation is due to the decreased precipitation contribution owing to the reduced precipitation cross section. With increasing strain range, the dislocation density increases; severe dislocation interaction leading to dislocation tangles have been observed in a specimen tested at Δε=2.0%. With such strong cyclic softening occurring in this strain range, it was expected that clear interaction between γ′ precipitates and dislocation deformation would be seen. However, the high deformation in this specimen made it impossible to see the diffraction contribution of γ′ phase, and therefore not possible to view their interaction.

As observed at room temperature, deformation by planar slip of dislocations was still predominant at 600°C and 800°C and stacking faults were readily seen. However, as temperature increased, more slip systems operated leading to frequent slip band intersection and dislocation tangles. Plastic deformation became more uniform and stacking fault lengths shortened. Small amounts of $M_{23}C_6$ carbides precipitated on dislocations and were coherent with matrix. The grain boundary carbides maintained coherency with one of their neighbouring grains. Slip systems were identified as $\{111\}\frac{a}{2}<110>$, as at room temperature. It appears that the gradual cyclic hardening at 600°C was due to the increased strength gained from more extensive dislocation interaction. Cyclic softening at 800°C is attributed to thermal activation allowing climb or cross slip process to overcome such interaction barriers.

The previous discussion on deformation mechanisms is supported by fractographic analysis. Scanning electron microscopy was used in failure analysis of fracture surfaces and cross sections of LCF tested specimens. It revealed that multi-crack initiation was the main feature in all specimens. At room temperature, cracks initiated by a transgranular localised slip process and fracture surfaces exhibited planar fracture characteristic. An example of such crack initiation and propagation sites is given in Fig. 8. When the temperature was increased to 800°C, a transgranular mode of crack initiation still persisted but a more wavy fracture surface was observed (Fig. 9), indicating a reduction in the planarity of slip. The fracture surface of the specimens tested at 600°C exhibited a mixture of the features shown at these two temperatures. It should be noted that creep cavitation at grain boundaries leading to intergranular fracture has been observed at 800°C for several stress levels [7]. The transgranular fracture mode and the lack of cavitation observed here indicate that in the present cycle waveform, fatigue played an important role in deciding the failure mechanism at 800°C.

Although C263 superalloy is designed for application at a temperature less than 800°C, it does experience temperatures as high as 950°C in service. At such temperature, it is expected that all the γ′ phase is dissolved as the solvus temperature of γ′ phase in C263 alloy is between 910-925°C [1]. When cooled down after LCF testing at 950°C, however, the specimen was found to contain dispersed γ′ phase in the matrix. In order to determine if precipitates were present at 950°C, a piece of C263 material, which was held at 950°C for 1.5h and then quickly air cooled, has been examined under TEM. No γ′ was observed after this treatment. The γ′ precipitates in the isothermal LCF tested specimen at 950°C were therefore simply due to the re-precipitation of γ′ phase during the slow cooling down process when the specimen failed.

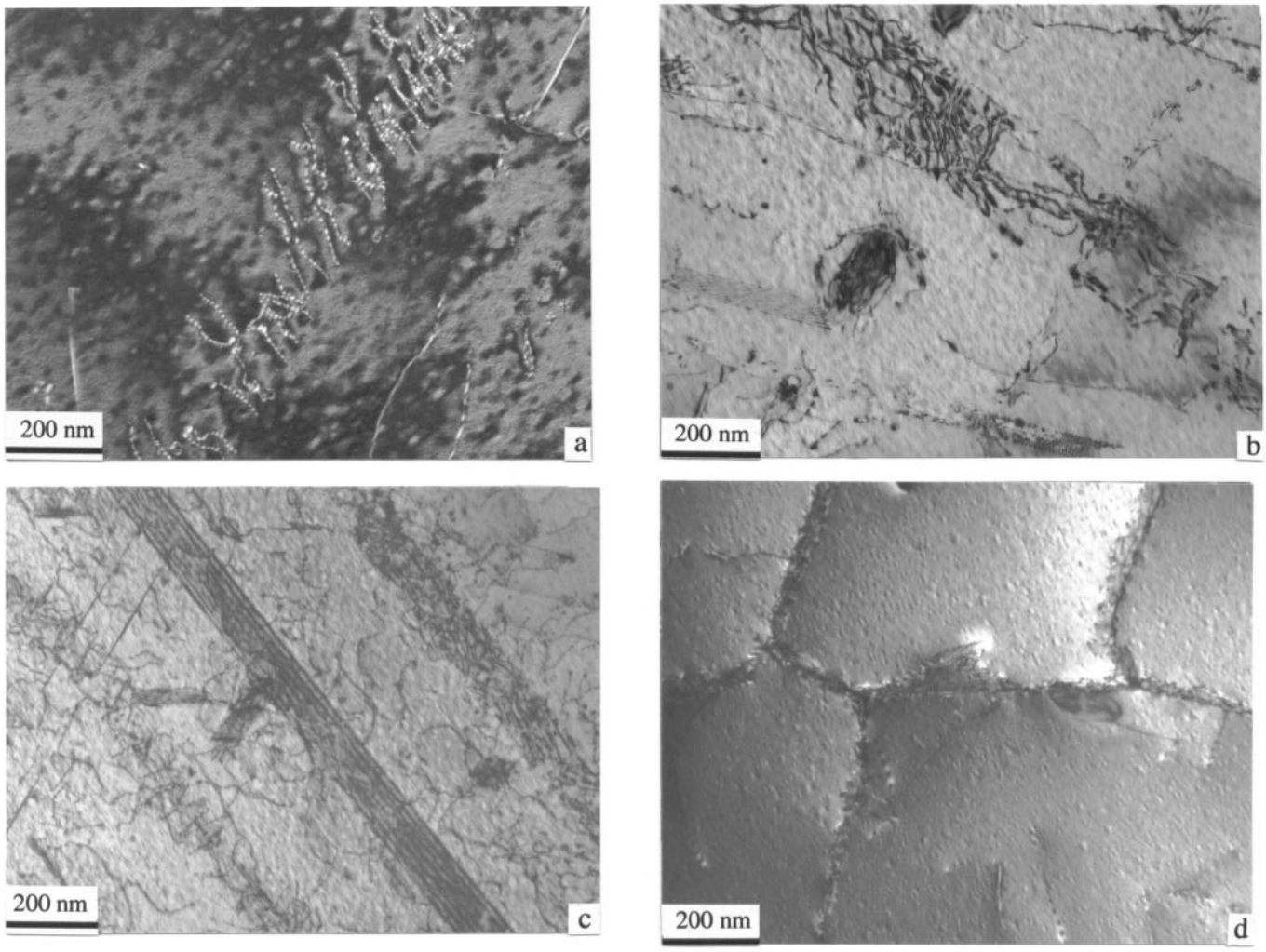

Figure 6: TEM micrographs illustrating the deformation microstructure at (a), room temperature, $\Delta\varepsilon$=0.75%, (b), 600°C, $\Delta\varepsilon$=0.75%, (c), 800°C, $\Delta\varepsilon$=0.75% and (d), 950°C, $\Delta\varepsilon$=0.50%.

After a short period of hardening for the majority of fatigue life slight softening was observed. At this temperature, the grain boundary $M_{23}C_6$ carbides became coarse and more discontinuous. In some regions, they lost their original coherency with neighbouring grains. Uniform dislocation distribution was observed within grains. The dislocation Burgers vector was still $\frac{a}{2}$<110>, and the majority of the dislocations observed were in the {111} planes, however some were found to reside on {100} planes. Dynamic recovery led to subgrains and cells. Secondary $M_{23}C_6$ particles precipitated preferably on subgrain boundaries and slip bands. One example of $M_{23}C_6$ carbides precipitating on slip bands is shown in Fig. 10 where these carbides precipitated in a linear fashion. Trace analysis of several such sites were carried out and found that these lines with carbide precipitates lay in {111} planes. Although these carbides can act as barriers to dislocation movement, it is unlikely that they can play a significant role in increasing the strength of the material because of their small quantity. Cavity induced cracks have been found at grain boundaries but failure initiated mainly from grain boundaries near specimen surfaces presumably because of the influence of oxidation, see Fig. 11, leading to intergranular fracture.

Thermomechanical Fatigue TEM observation of the OP TMF tested specimen in a longitudinal section revealed that the specimen has suffered from heavy plastic deformation. Elongated grain and sub-grains can be seen, Fig. 12. Heavy plastic deformation leads to recovery and recrystallization. Fig. 13 shows a grain boundary migrating towards a high density dislocation region, leaving behind original grain boundary carbides within a grain. Creep cavities were observed at grain boundaries indicative of their weakness during TMF, Fig. 14. Compared to the LCF specimen tested at 950°C, the dislocation density was higher and only a very small quantity of carbides was observed within grains. Fracture was primarily via an intergranular mode and was more prominent in IP TMF test.

Turbine components experience thermal and mechanical fatigue. Traditionally, design of these components against fatigue is based on the isothermal fatigue data at the highest temperature with the largest stress or strain. However, there is a strong likelihood that

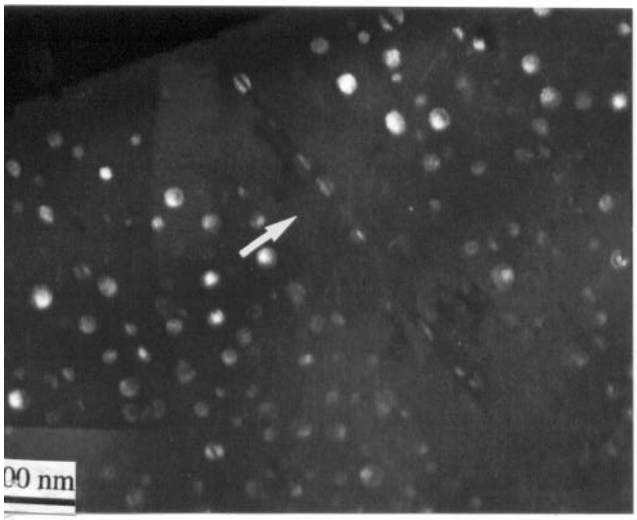

igure 7: TEM micrograph from room temperature LCF tested ecimen, showing sheared γ′ precipitates in the slip band rrowed), Δε=0.75%.

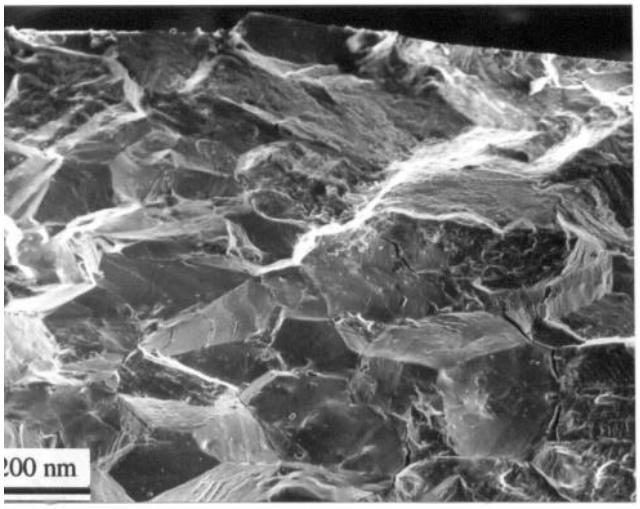

igure 8: SEM fractograph showing trangranular cleavage crack nitiation and propagation characteristics at room temperature, ε=0.75%.

ıe deformation mechanisms are different under TMF which cast oubt over the feasibility of above methodology. The difference etween isothermal fatigue and TMF both macroscopically and icroscopically have been found in other combustion materials 2,3]. Present TMF tests revealed the following differences in icromechanisms in deformation from LCF at 950°C: 1. High ensity dislocations and recrystallization. In TMF testing, because f severe creep deformation at high temperature, large reversed lastic deformation occurred at lower temperature causing a high ensity of dislocations. When the specimen was heated to high mperature, those heavily deformed regions either recovered or crystallized, leading to elongated grains or subgrains; 2. Carbide recipitation. In isothermal fatigued specimen at 950°C, many arbides precipitate within grains. They can act as barriers for islocation movements leading to precipitation hardening although

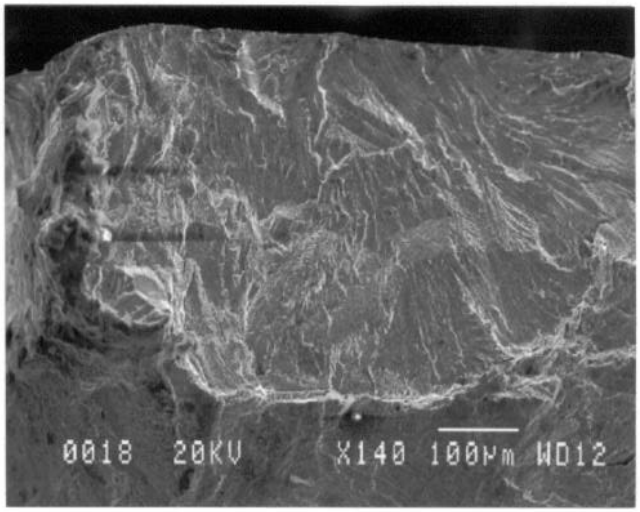

Figure 9: SEM fractograph showing quasi-cleavage fracture surface seen in isothermal LCF at 800°C, Δε=0.75%.

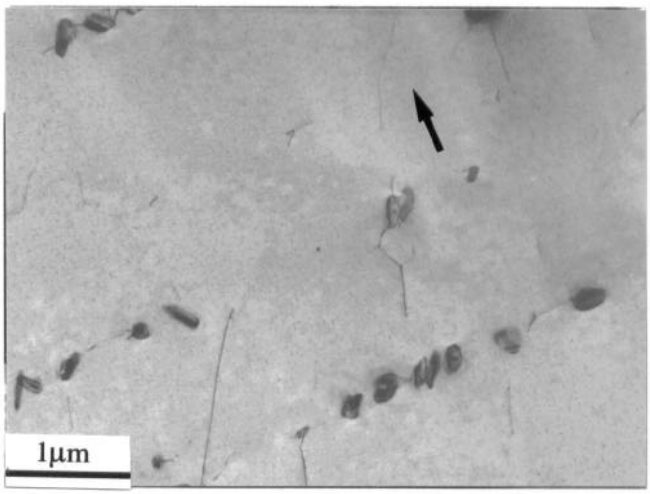

Figure 10: TEM micrograph showing $M_{23}C_6$ carbides precipitating along {111} slip bands in lines during isothermal LCF at 950°C (Δε=0.5%), **g**=111 (arrow direction).

their contribution might not be significant due to their small quantity. In the TMF specimen, little such carbide precipitation was observed. This is probably because of the shorter exposure time of the specimen to higher temperature during a TMF test.

Furthermore, solutionising of the microstructure in a TMF test might be the reason for the stress discontinuity seen in TMF tests. The phenomenon of dynamic strain ageing occurs in solid solutions where solute atoms are particularly free to diffuse through the parent lattice. It is preferable for these either interstitial or substitutional solutes to occupy sites in the vicinity of dislocations where they form Cottrell atmosphere around dislocations and hinder their movement. Since the microstructure of TMF tested specimens exhibited a solutionised structure with solute atoms dissolved in the γ matrix, it is not unexpected that dynamic strain ageing occurs during TMF. Indeed, in a similar

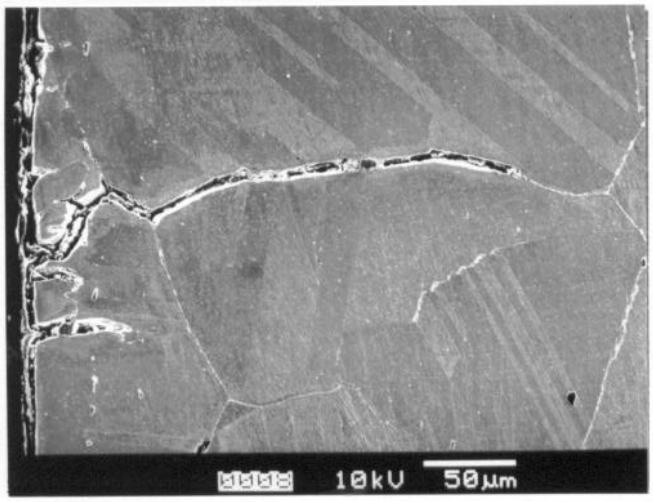

Figure 11: SEM micrograph taken from the cross section of a LCF tested at 950°C with $\Delta\varepsilon$=0.5% showing intergranular cracking from specimen surface.

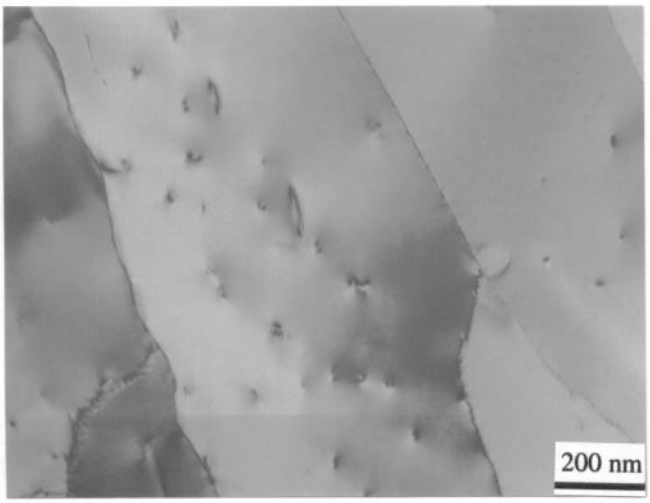

Figure 12: TEM micrograph showing elongated grain and subgrain structure developed during OP TMF.

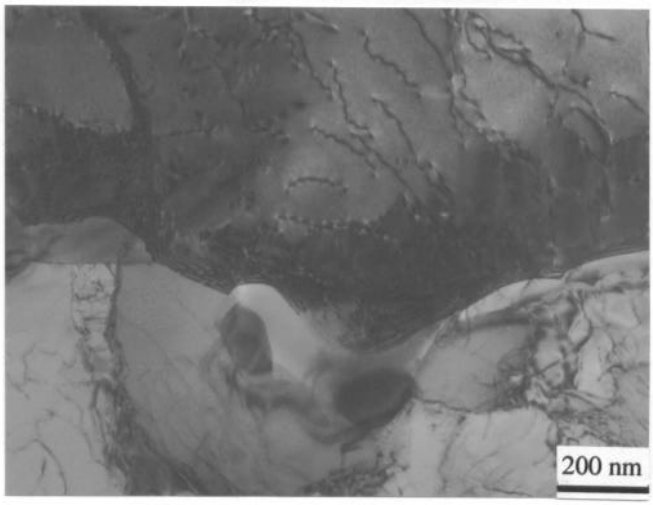

Figure 13: TEM micrograph showing shift of a grain boundary (upwards) during OP TMF. It moves towards a heavily deformed region, leaving original grain boundary carbides behind within a grain.

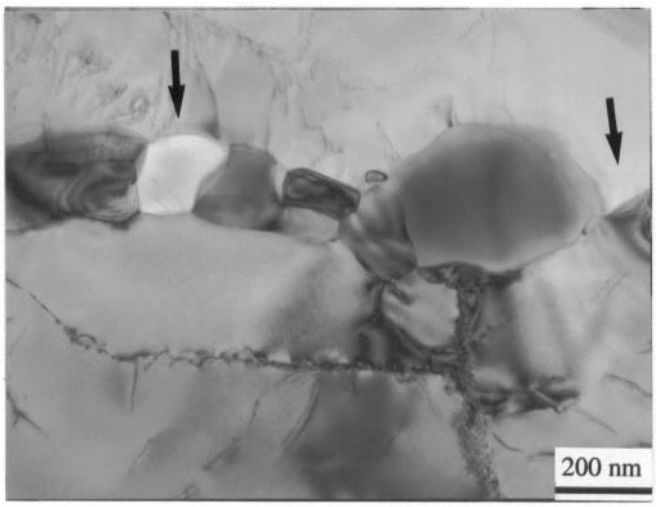

Figure 14: TEM micrograph showing cavity formation at a grain boundary during OP TMF.

superalloy, it has been found that the precondition for the appearance of dynamic strain ageing (discontinuous yielding) is that the maximum temperature must be high enough [8]. Although RF induction heating can induce a significant electrical noise leading to such stress fluctuation [9], it appeared that the stress discontinities are the true effect of dynamic strain ageing in the present study on the basis that the most severe stress discontinity occurred during cooling, the same observation as found in another material [8].

Conclusions

1, Initial cyclic hardening was observed at all tested temperatures in isothermal fatigue. It took less cycles to reach stress saturation with increasing temperature.

2, Cyclic hardening/softening depends on temperature. Hardening and softening was observed at 25°C, the levels being dependent on the strain range. At 600°C continual hardening occured. At 800°C and 950°C there was very limited hardening. Softening at 800°C was significant, but at 950°C the material was essentially cyclically stable with the stress bearing capacity significantly reduced.

3, Dislocation planar slip is predominant at temperatures up to 800°C. More slip systems operate with increasing temperature. Wavy slip occurred at 950°C and plastic recovery produced subgrains and cells.

4, TMF tests exhibit different deformation mechanisms from isothermal fatigue. High temperature creep deformation leads to

heavy low temperature plasticity, which in turn results in significant recovery and recrystallization during the next cycle.

5, Fracture is mainly transgranular from room temperature up to 800°C in isothermal LCF. It became predominantly intergranular in TMF and isothermal LCF at 950°C.

Acknowledgements

The authors wish to thank EPSRC for financial support for Y.H.Z. and Rolls-Royce Plc for the provision of materials. Helpful discussions with Mr. S. Williams (Rolls-Royce) are appreciated. The provision of laboratory facilities in the Department of Materials Science and Metallurgy at the University of Cambridge by Professor A.H. Windle is acknowledged.

References

1. W. Betteridge and J. Heslop ED., The Nimonic Alloys (Edward Arnold Publishers Limited, London 1974), 18.

2. M.G. Castelli, and K.B.S. Rao, "Cyclic Deformation of Haynes 188 Superalloy Under Isothermal and Thermomechanical Loadings", Proceedings of the 8th International Symposium on Superalloys, ed. R.D. Kissinger, D.J. Deye, D.L. Anton, A.D. Cetel, M.V. Nathal, T.M. Pollock and D.A. Woodford, (Warrendale, PA: The Metallurgical Society AIME, 1996), 375-382.

3. M.G. Castelli, R.V. Miner and D.N. Robinson, "Thermomechanical Deformation Behavior of a Dynamic Strain Ageing Alloy, Hastelloy X", Thermomechanical Fatigue Behaviour of Materials, ed. H. Sehitoglu (ASTM STP 1186, Philadelphia, 1993) 106-125.

4. V.S. Sarma, M. Sundararaman and K.A. Padmanabham, Effect of Size on Room Temperature Low Cycle Fatigue Behaviour of a Nickle Base Superalloy, Materials Science and Technology, 14 (1998) 669-675.

5. M. Valsan, D. Sundararaman, S.K. Ray and S.L. Mannan, "Low Cycle Fatigue Deformation Behaviour of a Nimonic PE-16 Superalloy in a Double-Aged Microstructural Condition", Trans. Indian. Inst. Met., 49 (1996) 471-477.

6. B.A. Lerch and V. Gerold, "Room Temperature Deformation Mechanisms in Nimonic 80A", Metall. Trans., 18A (1987) 2135-2141.

7. Y.H. Zhang and D.M. Knowles, "Micromechanism of Creep Deformation of C263 Superalloy" (Interim Report 2/AT29, UTC, Department of Materials Science and Metallugy, Cambridge University, Jan. 2000).

8. B. Kleinpass, K.H. Lang, D. Lohe and E. Macherauch, "Thermal-Mechanical Fatigue Behabiour of NiCr22Co12Mo9", Fatigue Under Thermal and Mechanical Loading, ed. J. Bressers, L. Remy and M Steen and J.L. Valles (Kluwer Academic Publishers, The Netherlands, 1996) 327-337.

9. M.G. Castelli and J. Ellis, "Thermomechanical Fatigue Behaviour of Materials", ed. H. Sehitoglu (ASTM STP 1186, American Society for Testing and Materials, Philadelphia, 1993), 195-211.